

Unconventional magnetoresistance and spin gapless semiconductor-like behavior across the Martensitic transformation in off-stoichiometric Co-Fe-Ti-Si Heusler alloy thin films

Mainur Rahaman,¹ Lanuakum A Longchar,¹ Rajeev Joshi,² R. Rawat,²
Archana Lakhani,² M. Manivel Raja,³ S. N. Kaul,¹ and S. Srinath^{1,*}

¹*School of Physics, University of Hyderabad, Hyderabad - 500046, Telangana, India*

²*UGC - DAE Consortium for Scientific Research, Indore-452001, India*

³*Defence Metallurgical Research Laboratory, Hyderabad-500058, Telangana, India*

In this work, the effect of anti-site disorder on magnetic, electrical resistivity, transverse magnetoresistance (MR_{\perp}), and anomalous Hall resistivity of off-stoichiometric Co-Fe-Ti-Si (CFTS) Heusler alloy thin films, with a particular focus on martensitic phase transformation and spin gapless semiconductor (SGS)-like behavior, is investigated. These thin films were grown on Si (100) substrate at different substrate temperatures (TS) ranging from 200 °C to 550 °C using magnetron sputtering, enabling control over the degree of anti-site atomic ordering from disordered $A2$ to ordered $L2_1$. All the films, irrespective of their disorder, exhibit a distinct thermal hysteresis and significant drop in resistivity, crossover from asymmetric to symmetric magnetoresistance (MR_{\perp}), and a sharp increase in MR_{\perp} around 300 K, confirming the occurrence of a thermo-elastic martensitic phase transformation (MPT). Detailed analysis of resistivity data indicates that for TS200 and TS350 films, a SGS based two-channel model describes the conductivity in the martensite phase, whereas TS450, TS500, and TS550 films, exhibit a usual metallic behavior with a resistivity minimum at low temperatures. All the CFTS films show soft ferromagnetic nature and follow the spin-wave equation up to 390 K, suggesting that $T_c \gg RT$. The saturation magnetization and Hall conductivity increase with increasing crystalline order. The scaling relation between the longitudinal resistivity and the anomalous Hall resistivity in the martensite phase reveals that skew scattering is the dominant scattering contribution in disordered films. A change in charge carrier type from hole to electron around the martensitic transformation temperature (~ 300 K) further supports the presence of SGS-like features in disordered films. The asymmetric MR_{\perp} , persistent up to room temperature, highlights the potential of these films for spintronic applications such as spin valves.

Keywords: Martensitic phase transformation, Heusler alloy, Spin valve, Spin gapless semiconductor, Anomalous Hall effect

I. INTRODUCTION

Heusler alloys, a class of intermetallic compounds, have garnered significant attention due to their multifunctional properties such as half-metallicity (HM), Spin gapless semiconductor behavior (SGS), high spin polarization, large magnetoresistance (MR), tunable magnetic anisotropy, and shape memory effect (SME), which are crucial for next-generation spintronics applications [1–6]. Among them, the SHE associated with martensitic phase transformations (MPT) has been extensively explored in Ni-based Heusler alloys [7–16] for its applications in magnetic sensors and refrigeration technologies. The MPT induces internal strain, leading to the formation of several martensitic variants within the ferromagnetic material. The first-order nature of MPT results in thermal hysteresis, which manifests in several physical properties, such as magnetization and electrical resistivity.

While extensive research has been conducted on Ni-based Heusler alloys [7–16] for their SME and magnetic field-induced strain effects, recent investigations into Fe [17, 18] and Co-based Heusler compounds [19–28] have

further advanced the understanding of martensitic phase transitions (MPT) in these systems. Notably, MPT has been identified in off-stoichiometric Co-Ni-Ga [20, 21], Co-Fe-V-Ga [22], $\text{Co}_2\text{Cr}(\text{Ga},\text{Si})$ [23], $\text{Co}_2\text{V}(\text{Ga}/\text{Al}/\text{Si})$ [24–26], and Co-V-(Al, Ga, In) [27, 28] alloys. In these Co based systems, the MPT occurs near the ferromagnetic transition temperature and is confirmed through the thermo-mechanical properties, leaving a huge research gap about their electrical and magneto transport properties across the magnetic and structural transition. Given the strong influence of MPT on electrical and magneto-transport properties, it often manifests as thermal hysteresis, a sudden drop in electrical resistivity, and significant changes in magnetoresistance and anomalous Hall resistivity, observed in many Ni-based SMAs [9–16]. However, a comprehensive understanding of the role of off-stoichiometry and structural disorder in governing martensitic transformations in Co-based Heusler alloys remains elusive.

The advent of spin-gapless semiconductors (SGSs) within the realm of half-metallic Heusler-type ferromagnets marks a significant development in semiconductor spintronics [3, 4]. These innovative materials are characterized by a unique electronic band structure, featuring a semiconducting bandgap for minority spin carriers while allowing for a zero bandgap for majority spins at

* srinath@uohyd.ac.in

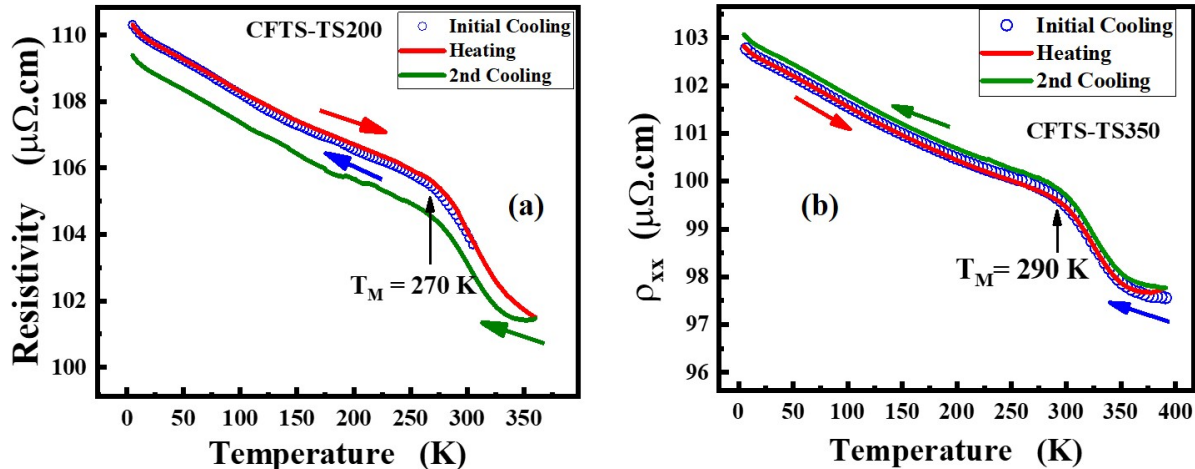


FIG. 1. Temperature-dependent zero-field resistivity for disordered TS200 and TS350 CFTS films in the cooling cycle (Blue circles/green lines) and the heating cycle (red lines).

Heusler-type SMAs [10–16]. Above the T_M , the austenite phase (AP) grows at the expense of the martensite phase (MP). Because of the instrumental limit on the upper most measurement temperature, $T_{meas} = 375$ K, the system does not fully transform into the austenite phase during the heating cycle. Instead, it stays in the mixed phase (martensite + austenite) in the temperature range $T_M \leq T \leq T_{meas}$. However, below T_M , the system is in the martensite phase. Irrespective of the magnitude of TS, all the films exhibit an upturn in resistivity (p-TCR) in the martensite-austenite mixed phase in the temperature range of 300 K to 330 K. Note that the T_C (~ 800 K) of these films is well above the T_M , with the result that both the martensite and austenite phases are in the ferromagnetic (FM) state (detailed magnetic behavior is presented in section C).

Compared to global probes such as magnetization [43–45], strain [46], and x-ray diffraction [47], especially in the case of thin films, local probes like electrical resistivity are often more reliable for detecting thermal hysteresis accompanying martensitic transformations because of their sensitivity to local structural changes. Martensitic transformations involve changes in the crystal structure that significantly affect electron scattering mechanisms, altering resistivity and making it a direct indicator of phase changes at the microscopic level. Thermal hysteresis, the difference in transformation temperatures during heating and cooling, can be captured more accurately by resistivity measurements because they respond directly to phase boundaries and associated structural changes. Global probes like magnetization might not show clear hysteresis if the magnetic properties of the ferromagnetic martensite and austenite phases do not differ significantly [11, 43–45].

The present disordered CFTS films (TS200 and TS350)

also have a high residual resistivity (RR) of $\sim 110 \mu\Omega\text{cm}$ (nearly double that of the ordered CFTS films) and exhibit n-TCR. This suggests that a very short mean-free path, due to substantial disorder, is linked to the small n-TCR. Chemical defects/impurities and the anti-site atomic disorder make these films a strongly disordered metallic system. The n-TCR observed in these CFTS systems can, in principle, be understood in terms of the Mooij correlation [48] and its subsequently modified version [49], which empirically suggests that a disordered metallic system with RR greater than $150 \mu\Omega\text{cm}$ generally exhibits n-TCR.

The atomic disorder destroys half-metallicity, as a finite density of states (DOS) appears in the minority spin channel at E_F . The temperature-dependent resistivity for the disordered CFTS films is described by considering the two-carrier model proposed by Kharel et al. [36, 37] for a weakly disordered spin-gapless semiconductor (SGS). According to this model, disordered SGSs feature majority spin channel exhibiting band overlap, while the minority spin channel displays a semiconducting band gap, as illustrated schematically in Fig.3. The conductivity (σ) of disordered SGSs is thereby represented as a sum of conductivities from both the overlapped channel (σ_1) and the semiconducting channel (σ_2).

$$\sigma = \sigma_1 + \sigma_2 = \sigma_0 \left[1 + 2 \ln 2 \left(\frac{k_B T}{g} \right) \right] + \sigma_{\text{SC}} e^{-\left(\frac{\Delta E}{k_B T} \right)} \quad (1)$$

where $g = \frac{D(E_F)}{b} = \frac{D(E_F)}{\frac{dD(E)}{dE}} \Big|_{E=E_F}$ is a parameter with the dimension of energy, and can have a positive or negative value depending on the sign of b (i.e., the energy derivative of the density of states (DOS) at E_F). ΔE is

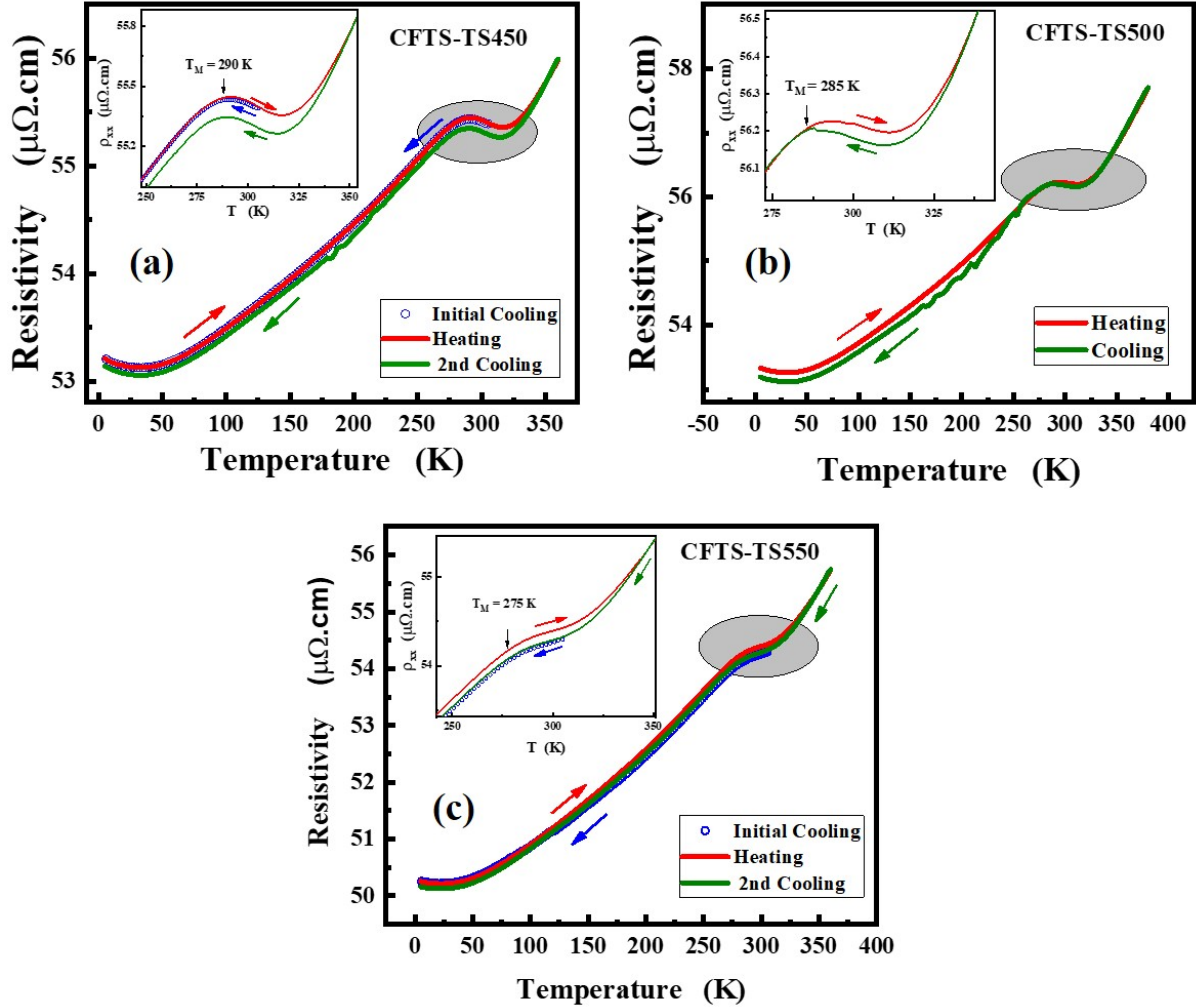


FIG. 2. Temperature-dependent zero-field resistivity for ordered TS450, TS500 and TS550 CFTS films in the cooling cycle (Blue circles/green lines) and the heating cycle (red lines).

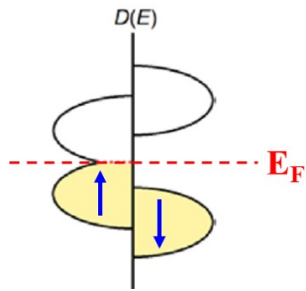


FIG. 3. A schematic illustration of disordered SGSs features one spin channel exhibiting band overlap, whereas the other channel displays a semiconducting band gap.

the gap in the semiconducting channel. Figure 4 demonstrates that the fits (green lines), based on the expression Eq. 1 yielded by the two-channel model, describe very

well the observed conductivity data (open dark circles) for the TS200 and TS350 CFTS films in the martensite phase. The corresponding resistivity data are shown in the insets. It is evident from the figure that conductivity is almost linear in the martensite phase, and therefore, the dominant contribution arises due to the SGS channel.

By contrast, the two-channel model is not applicable to the ordered crystalline ferromagnetic CFTS films TS450, TS500 and TS550 as they exhibit metallic behavior (Fig. 5) as opposed to the SGS or semiconducting behavior. The observed p-TCR is primarily due to electron-phonon ($e-p$) and electron-magnon ($e-m$) scattering mechanisms, which dominate at higher temperatures. However, due to the small residual atomic anti-site disorder present in the TS450, TS500 and TS550 CFTS films, quantum corrections (QC), such as enhanced electron-electron interaction ($E EI$), electron-diffuson ($e-d$) scattering and weak localization (WL) effects become important, par-

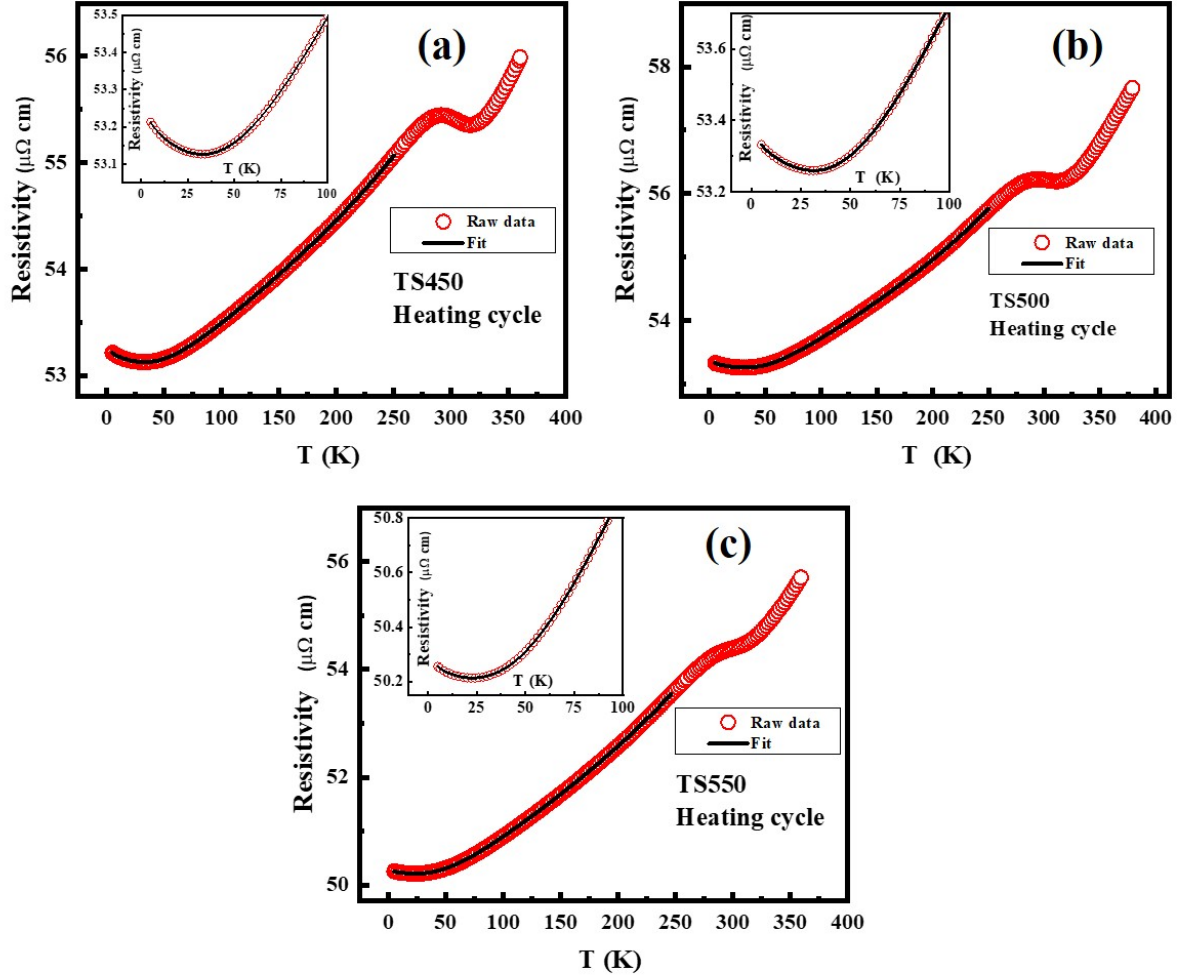


FIG. 5. Zero-field resistivity (red open circles) with theoretical fits (black solid curves) in the temperature range 5–250 K based on Eq.3 for TS450, TS500 and TS550 films. Insets: the enlarged view of the resistivity data with the fit in the low temperature.

TABLE I. Fit parameters for the best fit to the $\rho_{xx}(T, H = 0)$ data, based on the Eq.3, and T_{min} values for TS450, TS500 and TS550 films are also included.

CFTS films	ρ_{xx0} ($\mu\Omega\text{cm}$)	δ_{dif} ($10^{-2} \mu\Omega\text{cm}$)	ξ_{w1} ($10^{-4} \mu\Omega\text{cm K}^{-3/2}$)	β_{e-m} ($10^{-5} \mu\Omega\text{cm K}^{-2}$)	D_2 (10^{-6}K^{-2})	α_{e-p} ($\mu\Omega\text{cm}$)	θ_D (K)	χ^2 (10^{-6})	T_{min} (K)
TS450	53.28(2)	3.8(1)	4.0(2)	1.93(9)	1.08(8)	6.98(5)	363(2)	1.5	33
TS500	53.37(4)	2.7(2)	5.0(3)	2.3(1)	1.4(1)	9.08(8)	376(2)	3.9	31
TS550	50.30(2)	2.9(1)	2.3(2)	1.91(9)	1.77(9)	9.4(6)	376(1)	2.15	23

Panel (a) of Figs. 6 and 7 shows $\text{MR}_{\perp}(H)$ calculated, at different temperatures for the TS200 and TS500 CFTS films (MR_{\perp} data for TS350 and TS450 are presented in Supplementary Material V, Fig. S7 and S8). Irrespective of the strength of the anti-site disorder, for all the films, $\text{MR}_{\perp}(H)$ isotherms show unconventional behavior in the martensitic phase ($10 \lesssim T \lesssim 300$ K) wherein it changes sign with H (i.e., asymmetric, similar to magnetization switching) and has a very small value ($\text{MR}_{\perp} \sim 0.1\%$). In sharp contrast, at and above

the onset of martensite phase transformation, $\text{MR}_{\perp}(H)$ has a relatively higher value ($\sim 0.6\%$) at $H = 90$ kOe and, barring very low fields ($H \sim 0$), $\text{MR}_{\perp}(H)$ does not change sign with the field and exhibits a positive linear (symmetric) behavior. In the martensitic regime ($10 \text{ K} \lesssim T \lesssim 300 \text{ K}$), at low fields ($H \approx \pm 15$ kOe), MR_{\perp} increases linearly with H for all the films. At higher fields in the range $15 \text{ kOe} \lesssim H \lesssim 90 \text{ kOe}$, MR_{\perp} exhibits a plateau with a small positive slope for the disordered CFTS films (TS200 and TS350) (see Figs. 6(a)

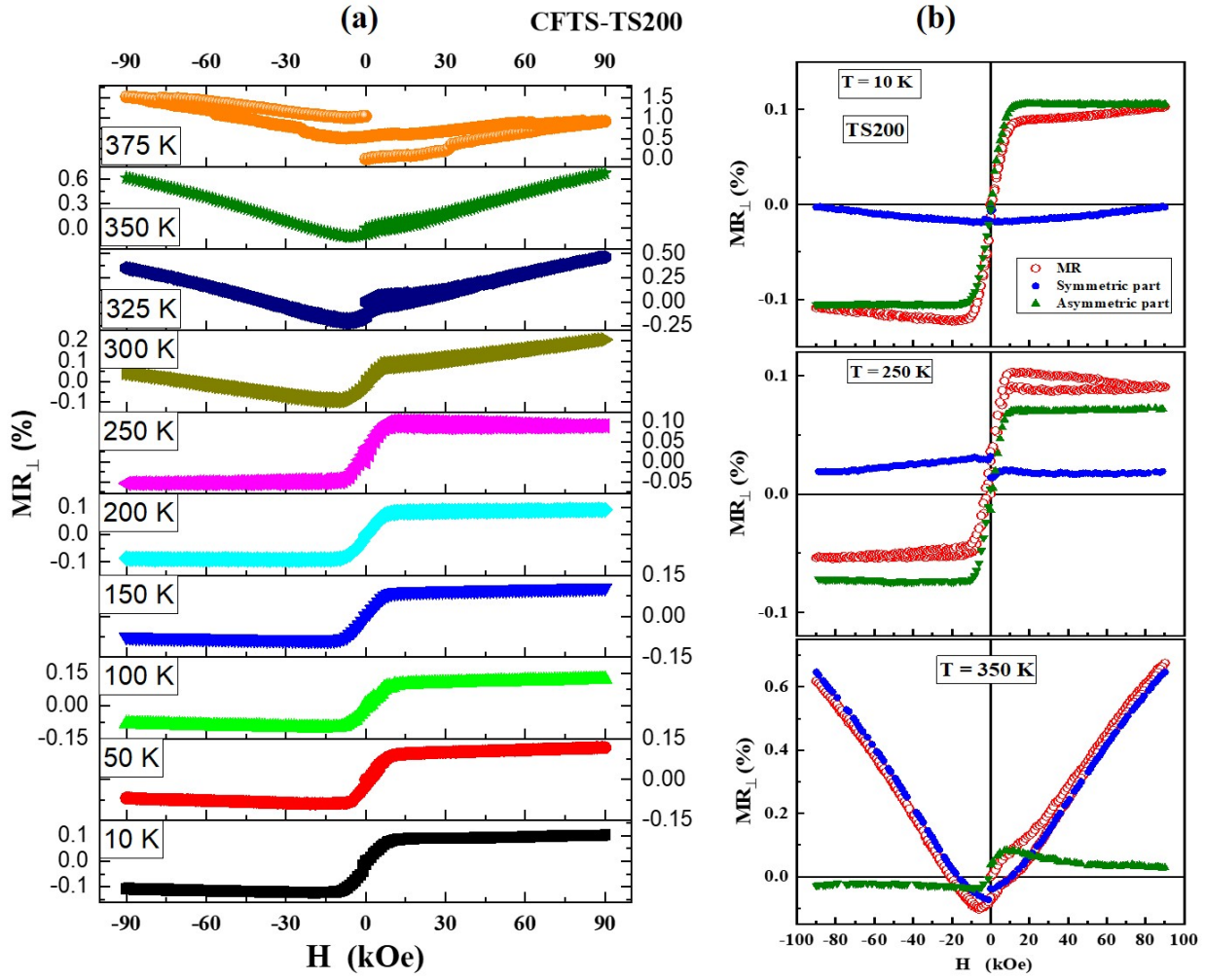


FIG. 6. (a) $MR_{\perp}(H)$ calculated at various temperatures for TS200 CFTS film. (b) Individual symmetric (red symbols) and asymmetric (blue symbols) parts of the actual MR_{\perp} behavior (green symbols) for 10 K, 250K and 350 K.

high-field ($H = 10$ kOe) and low-field ($H = 30$ Oe). A direct indication of the martensitic transformation in these films is not evident from M-T data (Fig. S1, Fig. 9), which shows only a narrow thermal hysteresis over a large range of temperatures. M-H hysteresis loops, recorded in both the martensite ($T = 5$ K) and austenite ($T = 350$ K) phases, as shown in Fig. 10(a)-(b) (Fig. S3), confirm the soft ferromagnetic nature of the CFTS films throughout the martensitic phase transformation. The saturation magnetization is higher in the martensite phase compared to the austenite phase for all films, and it increases with increasing crystalline order, i.e., substrate temperature, as demonstrated in Fig. 10(c).

The high field M-T data (cooling cycle) is analyzed using the well-known spin-wave (SW) expression [61, 73, 74]

$$M_S(T) = M_S(0) - g\mu_B \left[Z\left(\frac{3}{2}, t_H\right) \left(\frac{k_B T}{4\pi D_{sw}(T)} \right) \right]^{3/2} \quad (6)$$

where $M_S(0)$ is the saturation magnetization expected at the absolute zero of temperature, $Z\left(\frac{3}{2}, t_H\right)$ is the Bose-Einstein integral function and t_H is the dimensionless quantity related to the energy gap in the spin-wave spectrum arising from the effective field. $D_{sw}(T)$ is the spin-wave stiffness. Eq. 6 with the thermal renormalization of spin-wave stiffness given by $D_{sw}(T)$, yields the best fit to the $FC - M(T)$ data over the temperature range 50 K – 350 K. To optimize the SW fit, $M_S(0)$, D_0 and D_2 were treated as free-fitting parameters. Here, the thermal renormalization of D_{sw} due to the electron-magnon (D_2) term is crucial to reproduce the observed magnetization behavior, which is elucidated in Fig. S2 for a representative SW fit for TS350 film with D_2 as

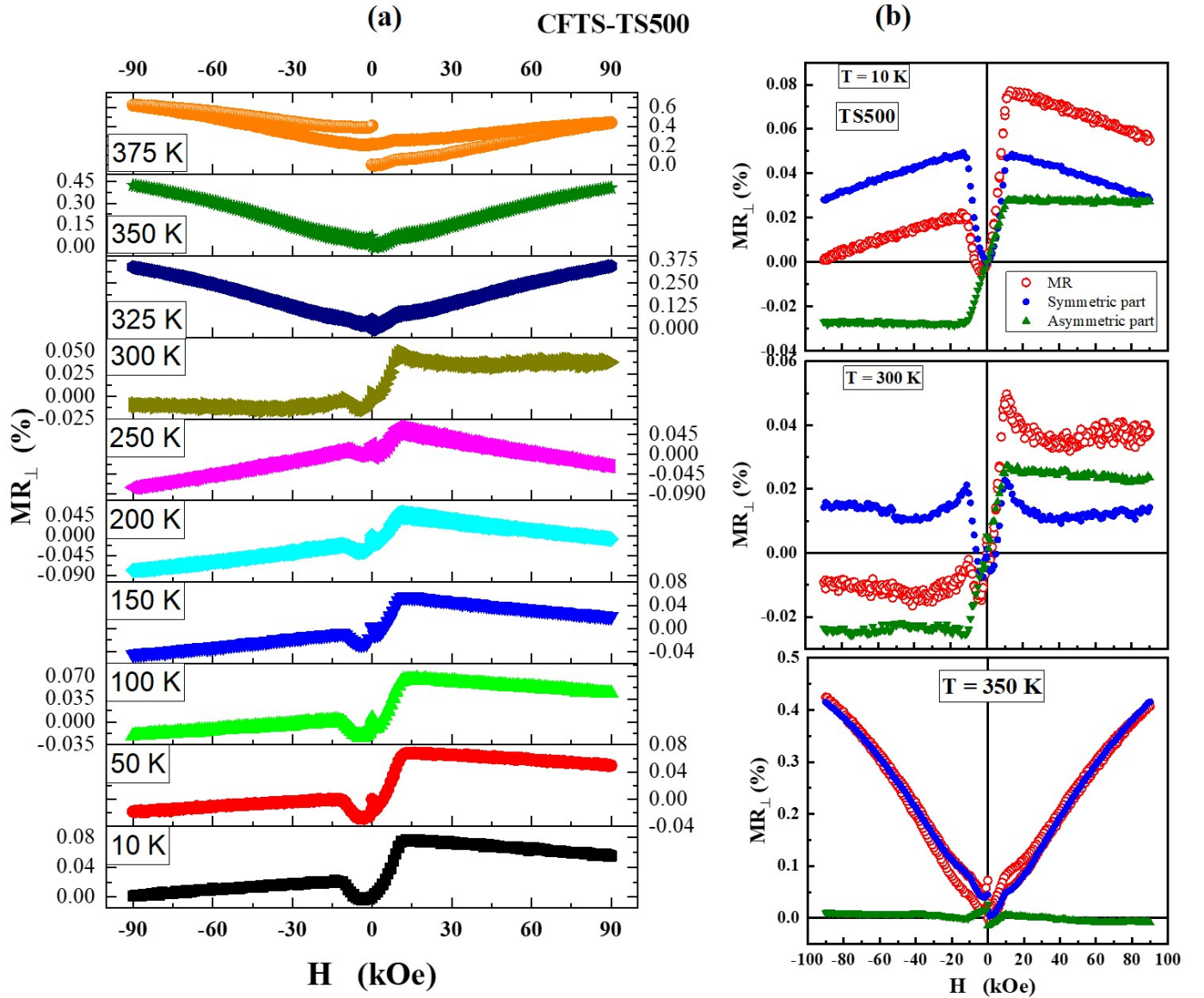


FIG. 7. (a) $MR_{\perp}(H)$ calculated at various temperatures for TS500 CFTS film. (b) Individual symmetric (red symbols) and asymmetric (blue symbols) parts of the actual MR_{\perp} behavior (green symbols) for 10 K, 250K and 350 K.

the free-fitting parameter, gives a better representation of the $M - T$ data compared to when the thermal renormalization of D_{sw} is not considered. In Fig. 9, solid blue lines denote the optimum SW fits. The SW fit is extrapolated up to 5 K by a blue dotted line shown in the inset of the respective figures. An anomalous softening of spin-wave modes in the martensitic phase could be a possible cause for the deviation from the SW fit and the upturn observed below $\approx 30K$ (Fig. 9) in the magnetization at low temperatures. The relevant SW parameter values are tabulated in Table II.

The M-H isotherms for TS200, TS350, TS450 and TS500 CFTS films were measured at various temperatures ranging from 5 K to 350 K. These isotherms are

corrected for the diamagnetic contribution of the silicon substrate, as depicted in Figs. S4 (a)-(d). The spontaneous magnetization at different temperatures ($M_{Sp}(T)$) is determined from the intercepts on the ordinate axis obtained by extrapolating the linear high-field regions of the $M - H$ isotherms to $H = 0$. The $M_{Sp}(T)$ data, so obtained, are fitted to the spin-wave (SW) expression, Eq.6. The optimum SW fits are depicted as red curves in Fig. S6.

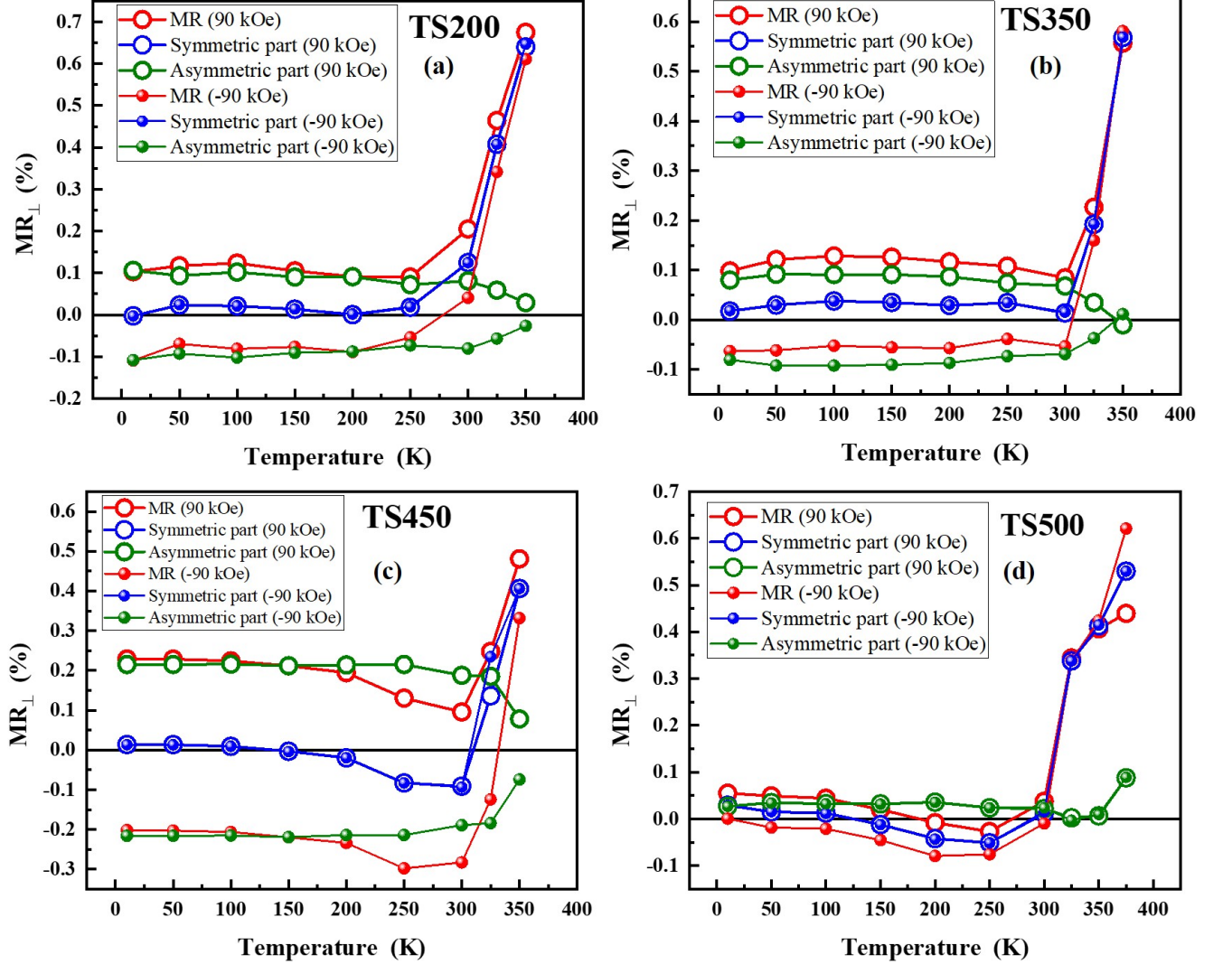


FIG. 8. Temperature variation of the magnitude of actual observed $MR_{\perp}(H)$, and its symmetric and asymmetric parts extracted at $\pm 90 kOe$ for TS200, TS350, TS450 and TS500 CFTS films

TABLE II. Values of the spin-wave (SW) parameters obtained from $M_{FC}(T)$ fit at 10 kOe; $M_S(0)$, D_0 and D_2 .

CFTS	$M_S(0)$ (emu/cc)	D_0 (meV·Å ²)	D_2 (10 ⁻⁶ K ⁻²)
TS200	758	108	0.65
TS350	763	115	0.79
TS450	1024	141	0.095
TS500	1025.6	144	0.003

D. Anomalous Hall Effect (AHE)

Figure 11 shows the Hall resistivity ($\rho_{XY}(H)$) data for the CFTS films at fixed temperatures in the range 5 K to 350 K and applied magnetic fields up to $\pm 50 kOe$.

As shown in this figure, the Hall resistivity initially increases rapidly with the magnetic field and nearly saturates at $H \sim 7 kOe$. $\rho_{XY}(H)$ isotherms mimic the $M(H)$ isotherms, shown in Fig. S4. The Hall resistivity is given by the expression [75–78]

$$\rho_{xy} = R_0 H + 4\pi M_S R_A \quad (7)$$

where R_0 and R_A represent the ordinary and anomalous Hall coefficients, respectively, M_S is the magnetization of the films. The ordinary Hall resistivity (ρ_{xy}^{OHE}), which is linearly proportional to H , arises from the Lorentz force, whereas the anomalous Hall resistivity ($\rho_{xy}^{AHE} = \rho_{xy}(H = 0) = 4\pi M_S R_A$) is linked to the intrinsic magnetization. ρ_{xy}^{AHE} at different temperatures

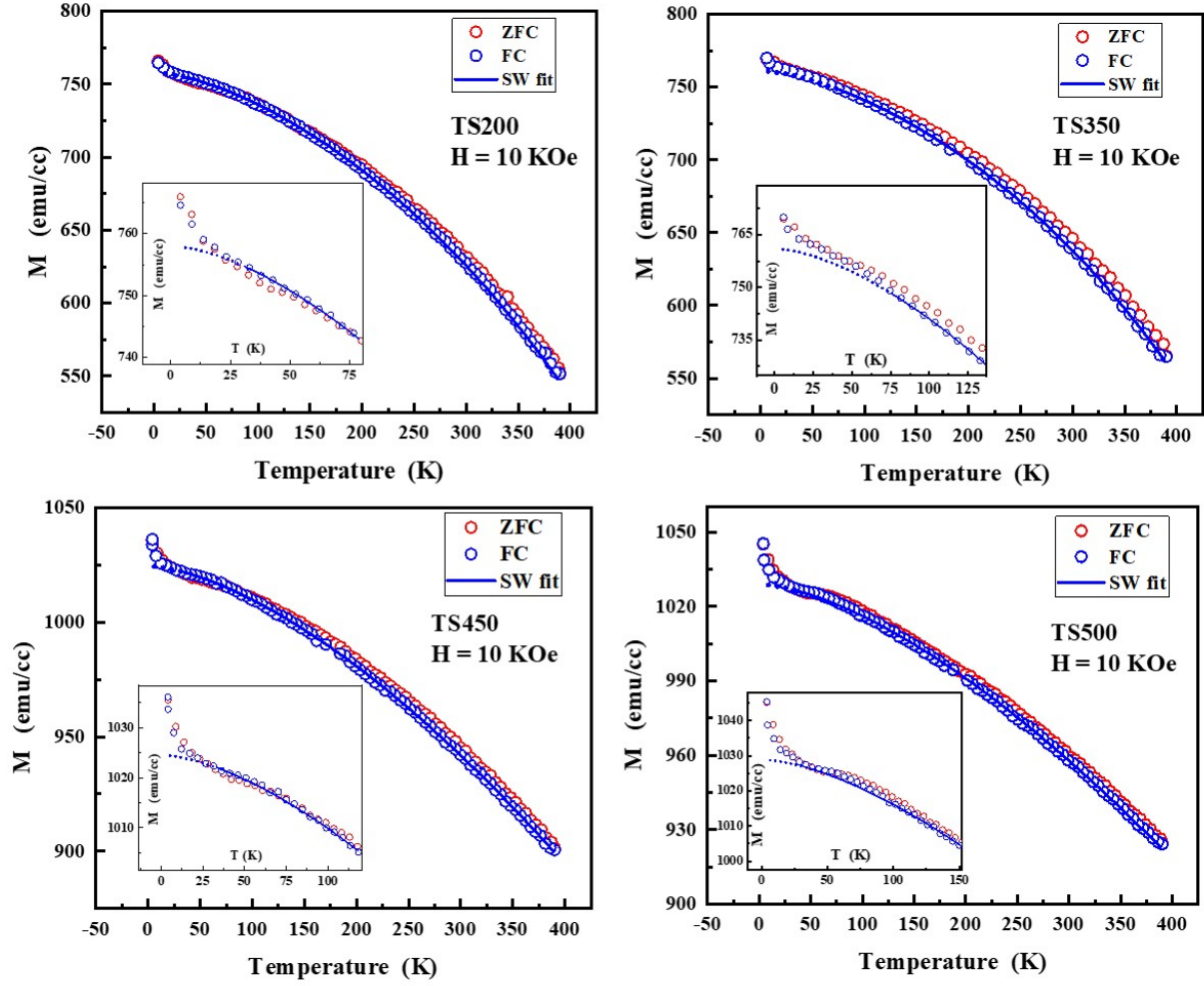


FIG. 9. $M - T$ curves for TS200, TS350, TS450 and TS500 CFTS films. Data recorded in both heating (ZFC) and cooling (FC) modes at $H = 10kOe$. Inset: highlights the low-temperature region where magnetization upturn is observed.

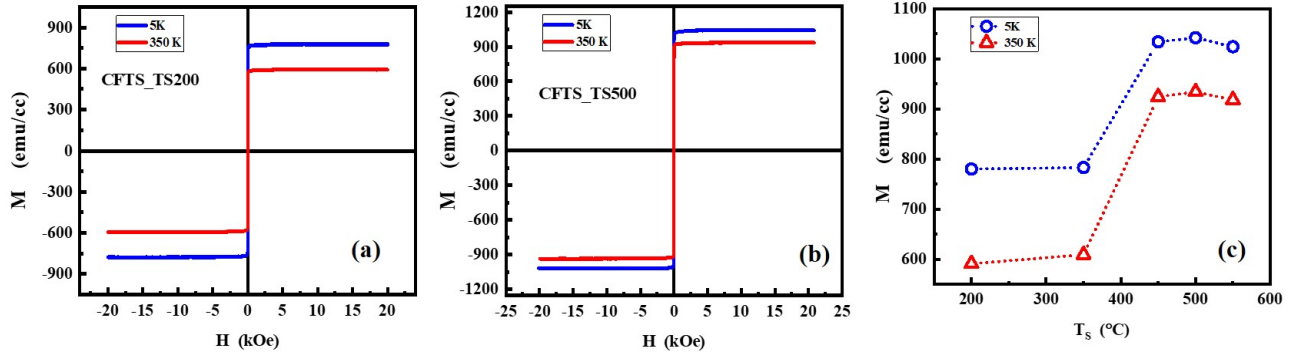


FIG. 10. (a)-(b) $M - H$ curves measured at different (a) temperatures for TS200 and TS500 CFTS films. (c): Variation of saturation magnetization with TS.

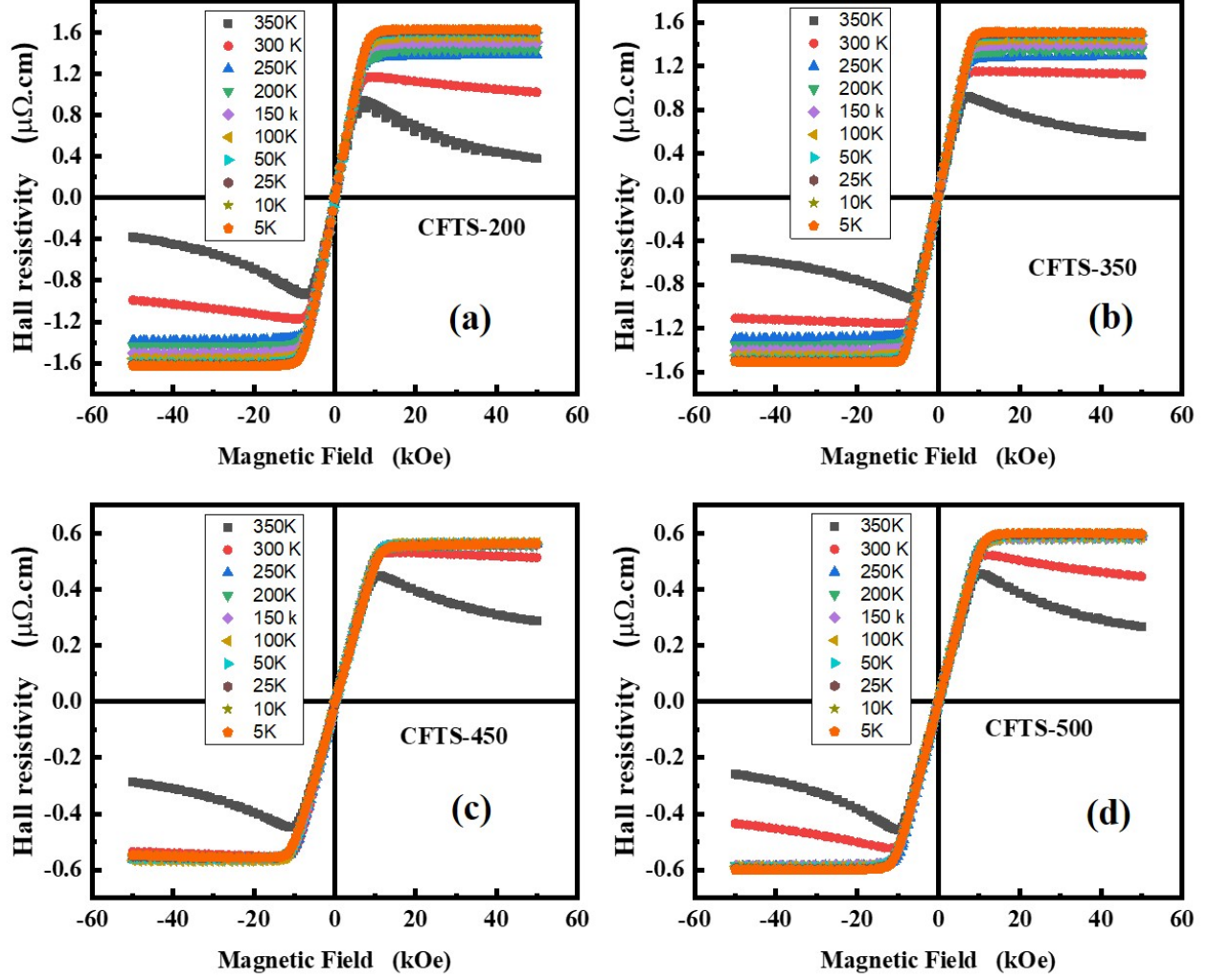


FIG. 11. (a)-(d) Hall resistivity as a function of field recorded at different temperatures for TS200, TS350, TS450 and TS500 CFTS films.

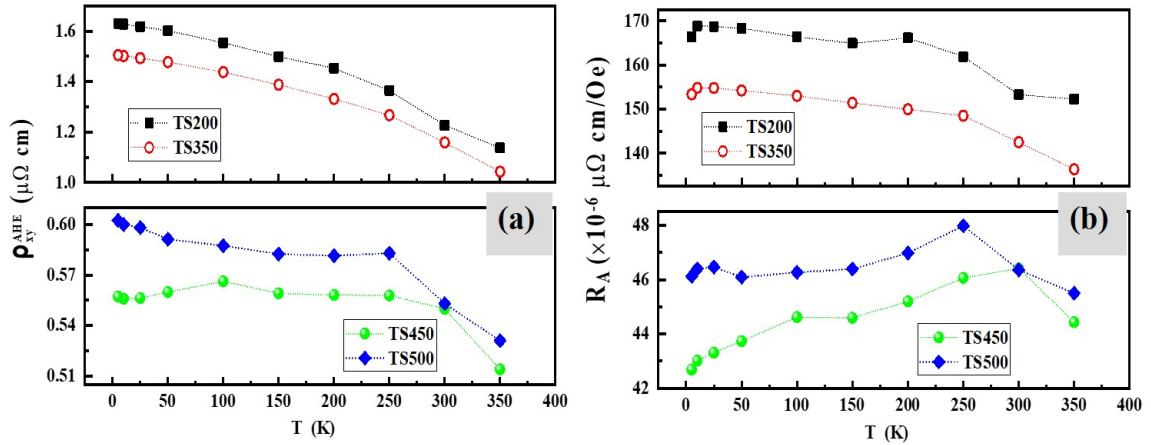


FIG. 12. (a) The temperature variations of ρ_{xy}^{AHE} and (b) $R_A(T)$ for for TS200, TS350, TS450 and TS500 CFTS films

